Electronic Supplementary Material (ESI) for Materials Advances.

Supporting Information

Chiral Amplification Induced by Self-Assembly of Different Aggregation States in Liquid Crystal Block Copolymer Films with Chiral Response

Jianan Yuan, [b] Xuemin Lu, *[a] Xiaojie He, [b] Feng Zheng, [b] and Qinghua Lu *[a]

[a.] *School of Chemistry and Chemical Engineering, Shanghai Jiao Tong University, Shanghai, 200240, China. E-mail: xueminlu@sjtu.edu.cn, qhlu@sjtu.edu.cn.*

[b.] *School of Chemical Science and Engineering, Tongji University, Shanghai, 200092, China.*

Results and Discussion

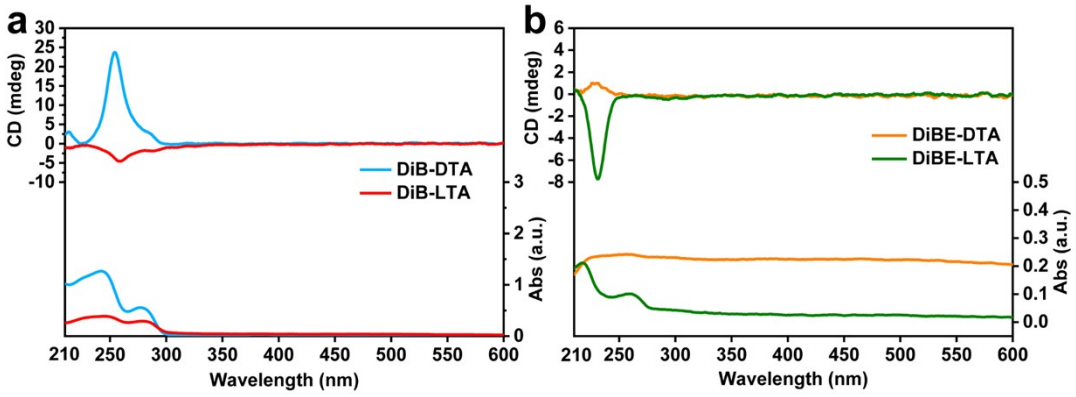

Figure S1. CD and UV-vis spectra of (a) DiB-D/LTA films and (b) DiBE-D/LTA.

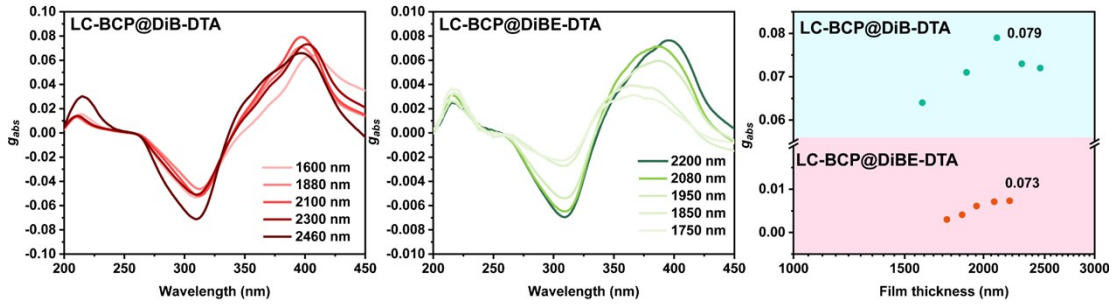

Figure S2. g_{abs} of LC-BCP@DiB-DTA annealed film and LC-BCP@DiBE-DTA annealed film with different thickness.

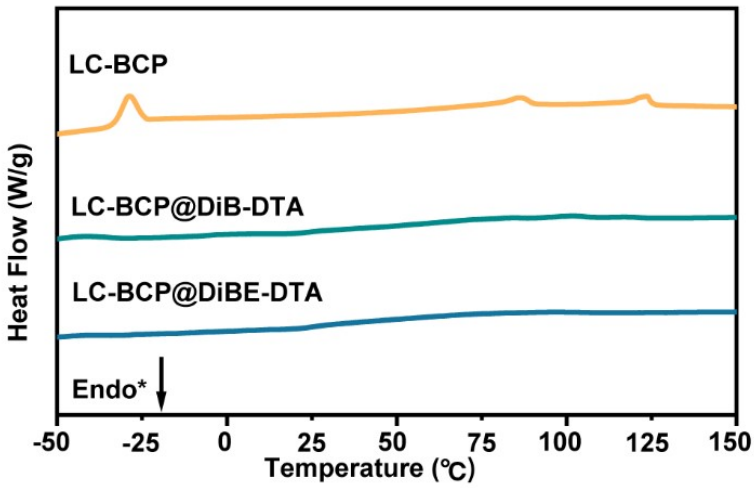

Figure S3. DSC cooling curve of LC-BCP, LC-BCP@DiBE-DTA, and LC-BCP@DiB-DTA.

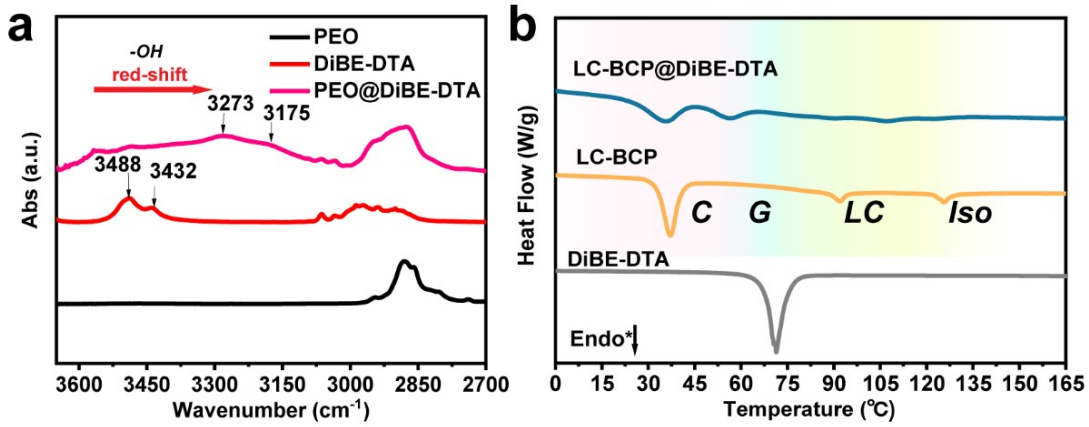

Figure S4. (a) IR spectrum of PEO, DiBE-DTA, and PEO@DiBE-DTA, respectively. The two peaks of -OH group of chiral molecules are red shift. (b) DSC heating curve of LC-BCP, DiBE-DTA, and LC-BCP@DiBE-DTA; C: crystalline phase; G: glass transition; LC: liquid crystal phase; Iso: isotropic phase.

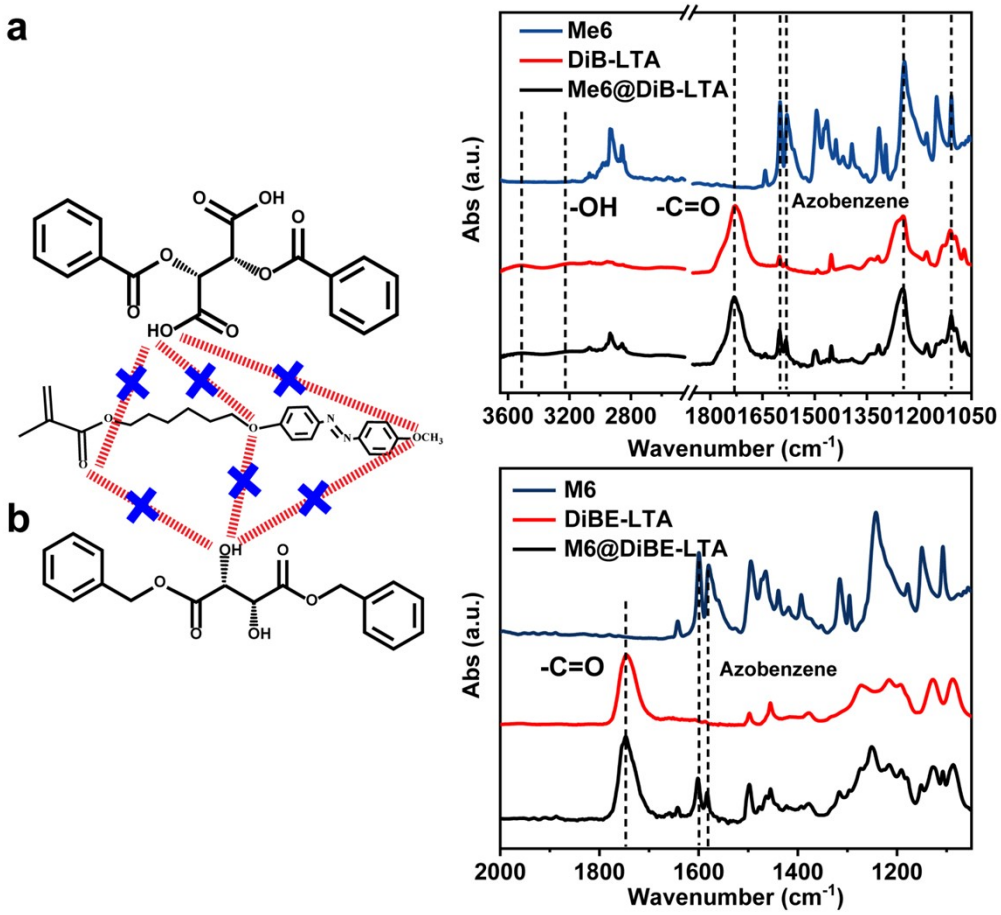

Figure S5. (a) IR spectrum of Me6, DiB-LTA, and Me6@DiB-LTA. (b) IR spectrum of Me6, DiBE-LTA, and Me6@DiBE-LTA.

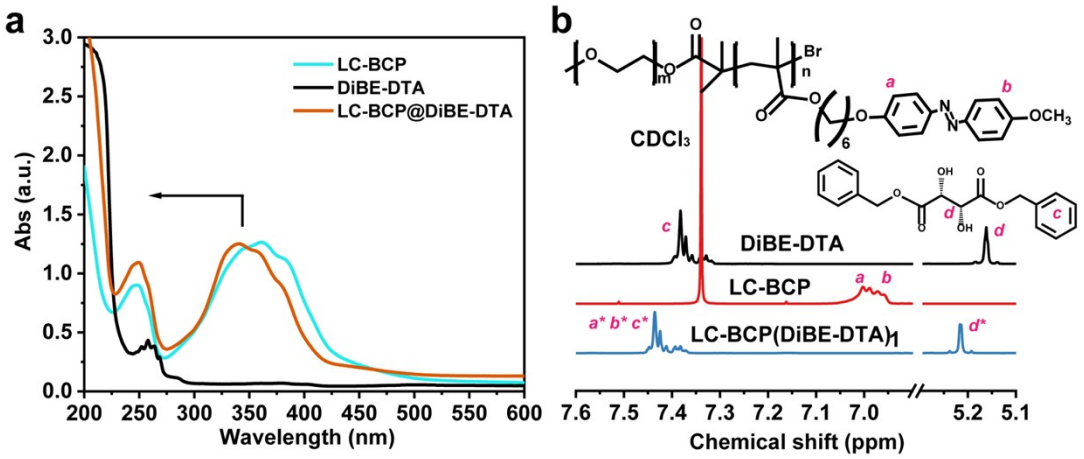

Figure S6. (a) UV-vis spectra of LC-BCP, DiBE-DTA, and LC-BCP@DiBE-DTA, (b) NMR spectra of LC-BCP, DiBE-DTA, and LC-BCP@DiBE-DTA with a molar ratio of 1.

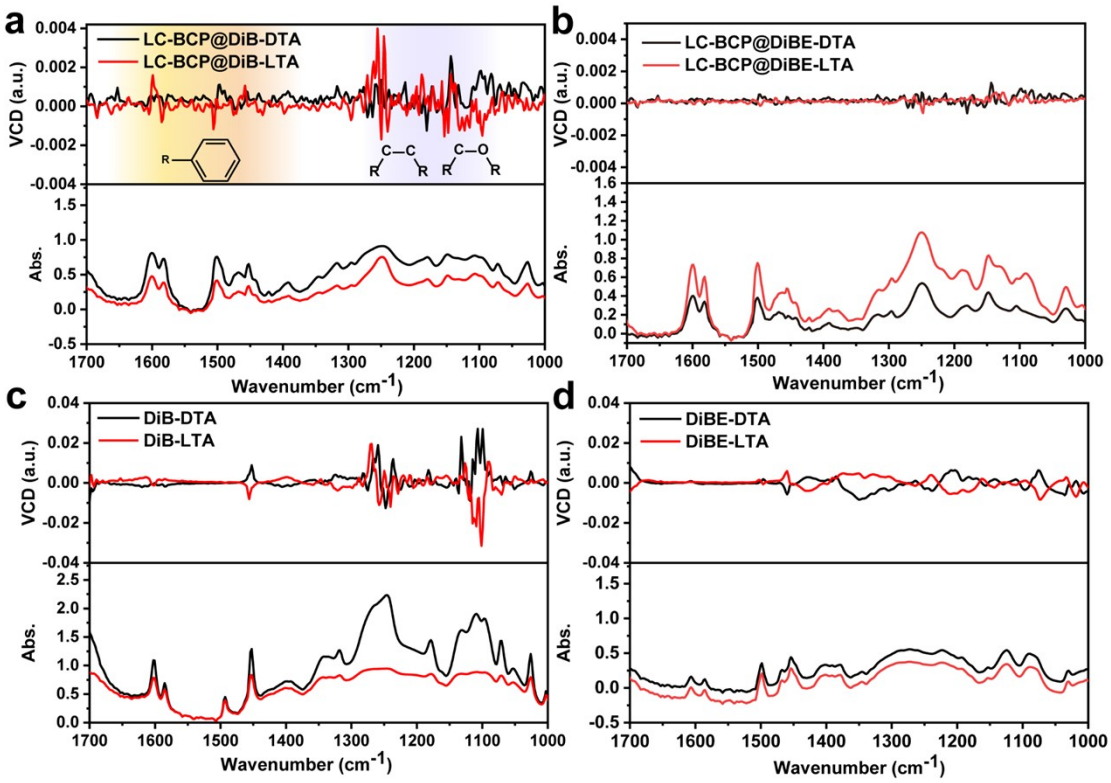

Figure S7. VCD spectra of LC-BCP@DiBE-D/LTA films (a), LC-BCP@DiBE-D/LTA films (b), DiB-D/LTA (c), DiBE-D/LTA (d).

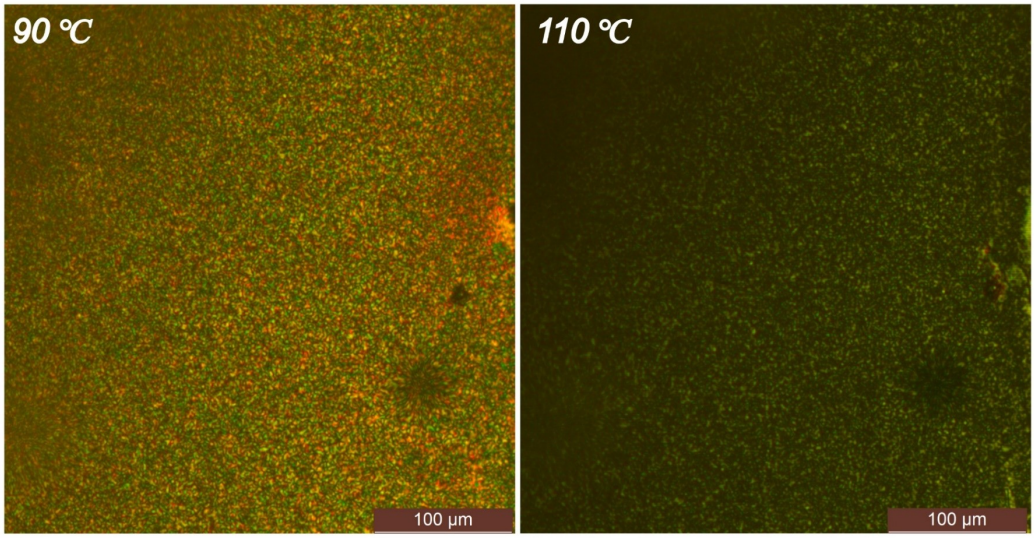

Figure S8. POM of LC-BCP@DiBE-DTA at 90 ºC (left) and 110 ºC (right).

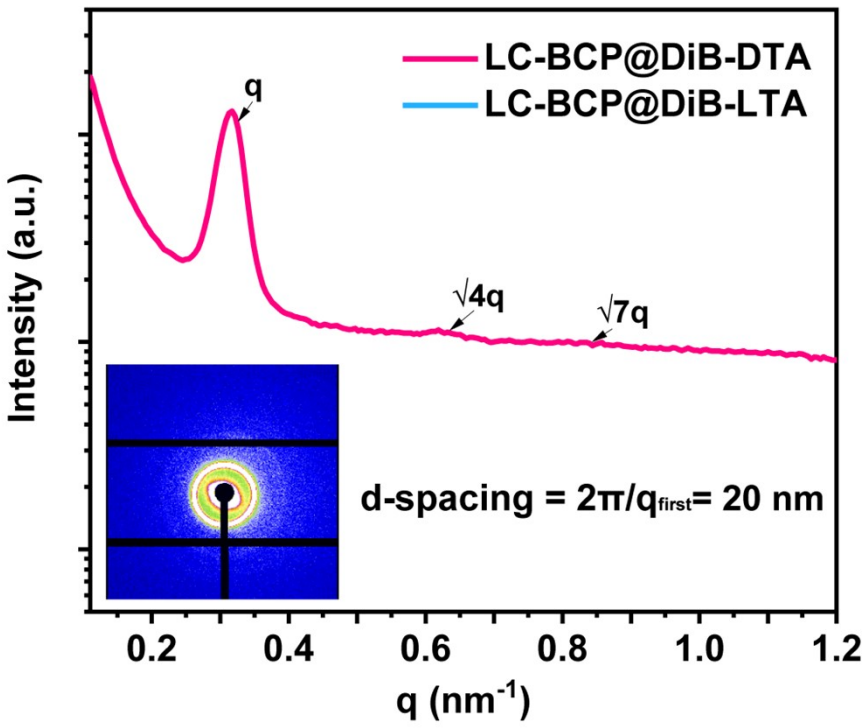

Figure S9. SAXS profiles of the annealed LC-BCP@DiB-DTA films. The image on the bottom is a two-dimensional diagram of SAXS.

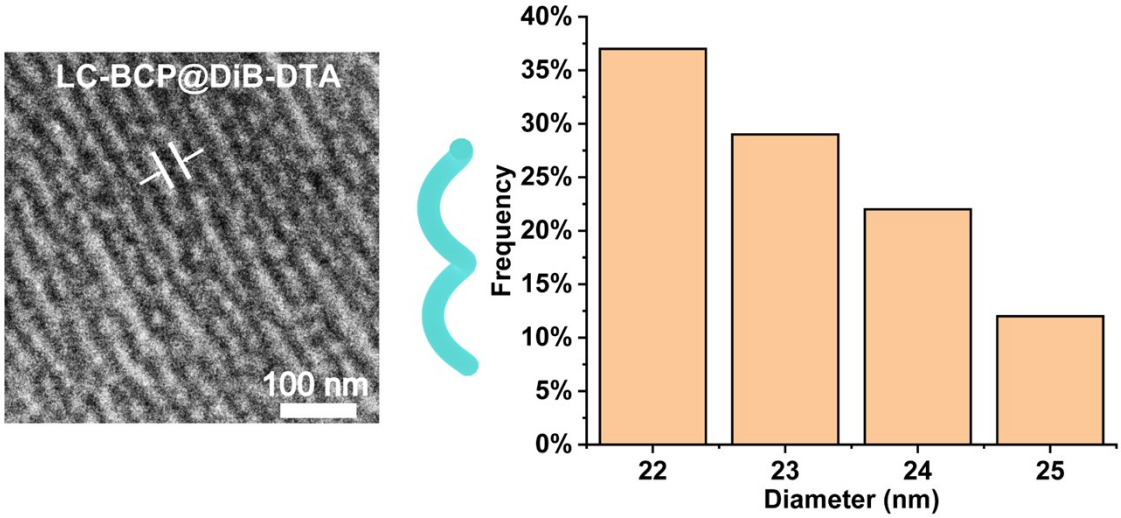

Figure S10. Bright-field images of LC-BCP@DiB-DTA films. The image on the right represents the helical diameter distribution.

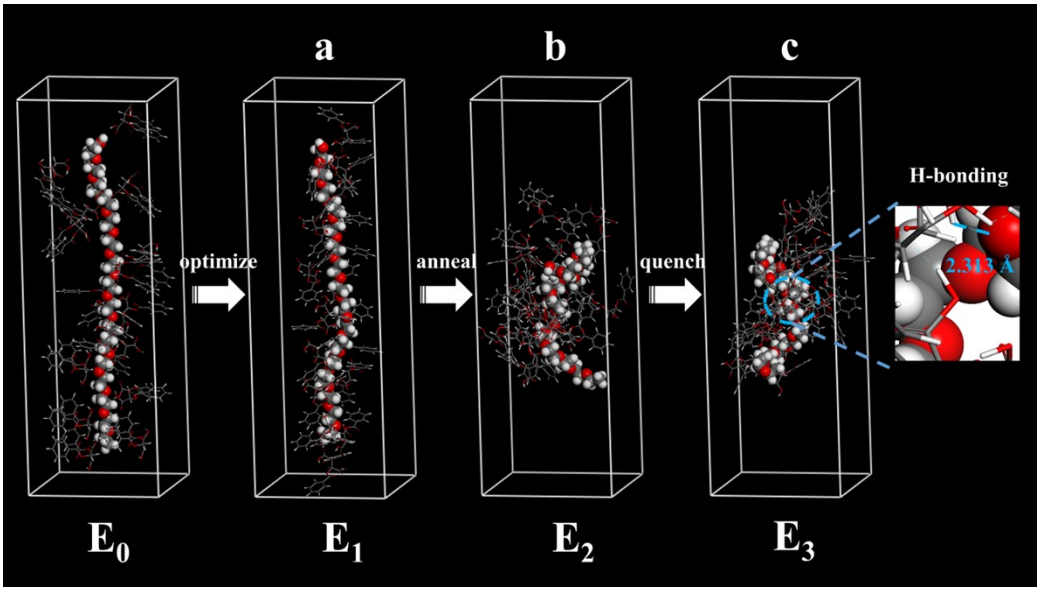

Figure S11. Energy-optimized structure (a), NVT and NPT annealing dynamic simulation (b), and quenching dynamic simulation (c). The inner diagram shows the H-bonding between the carboxyl group of the chiral molecule and PEO.

All dynamic simulations were performed in the Forcite module with the COMPASS Ⅱ force field.[1] To further explore the chiral induction mechanism of PEO@DiBTA, the PEO-DiBTA model was generated using the Amorphous Cell module.[2] To eliminate unreasonable local structures, the geometric optimization of the model used smart algorithms, and the maximum interaction was 50,000 steps. After 300 ps restricted NVT and 300 ps NPT pre-equilibrium, NVT annealing dynamic was performed with 15 cycles from 298 K to 398 K, and an annealing time of 600 ps. The temperature was held by a Nose-Hoovér thermo-stat.[3] All snapshots of the configurations were taken from the last 10 ps of simulation. The helical structure appeared locally, which was consistent with the experimental results. Then, a 400 ps quenching dynamic simulation was performed to obtain a more regular helical conformation. Inspired by the energy differences during the conformational changes of the small molecules[4] and the energies during changes in the mechanical behaviors of macromolecules,[5] we estimated different models based on the changes in the total energy. The helical conformation remained relatively stable. [6, 7]

Table S1. Comparisons of energies during different steps of the dynamic simulation.

structure	Random E_0	Simple optimized structure E_1	Annealing intermediate state E_2	Quenching steady state E_3
PEO@DiBTA	7883.38	100.03	237.07	-152.94

Units: kcal/mol

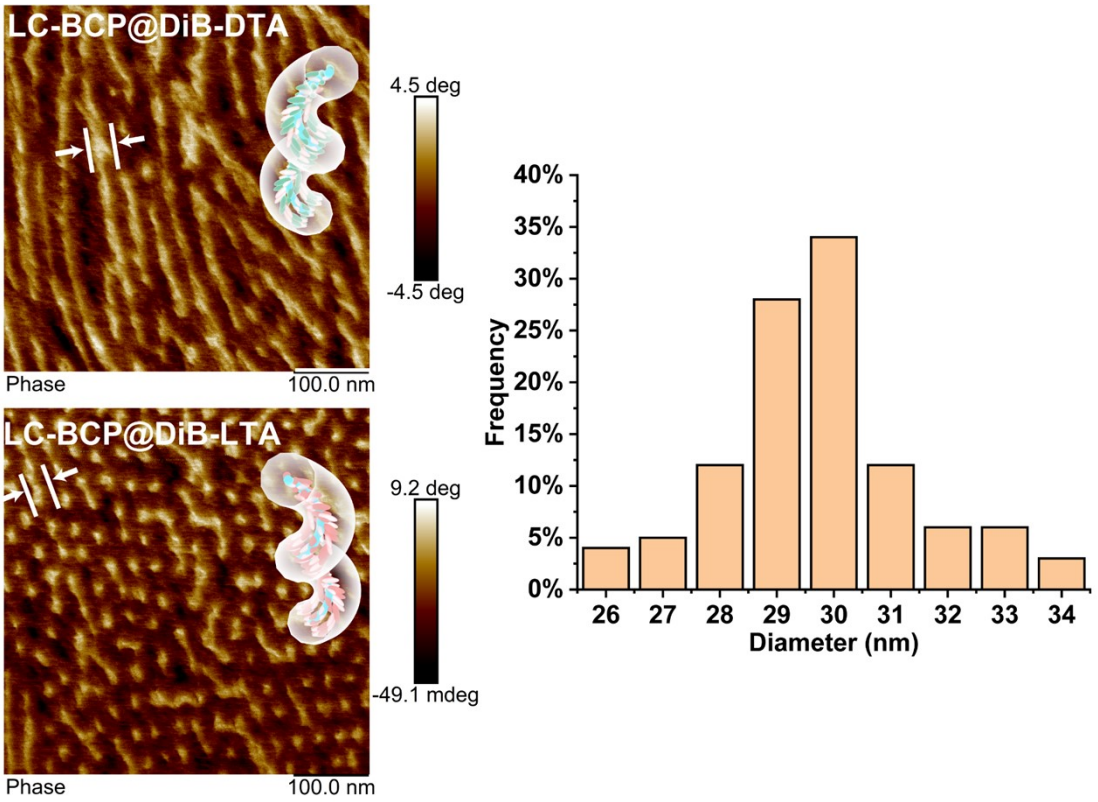

Figure S12. AFM phase images of LC-BCP films loaded with DiB-DTA and DiB-LTA. The picture on the right represents the helical diameter distribution.

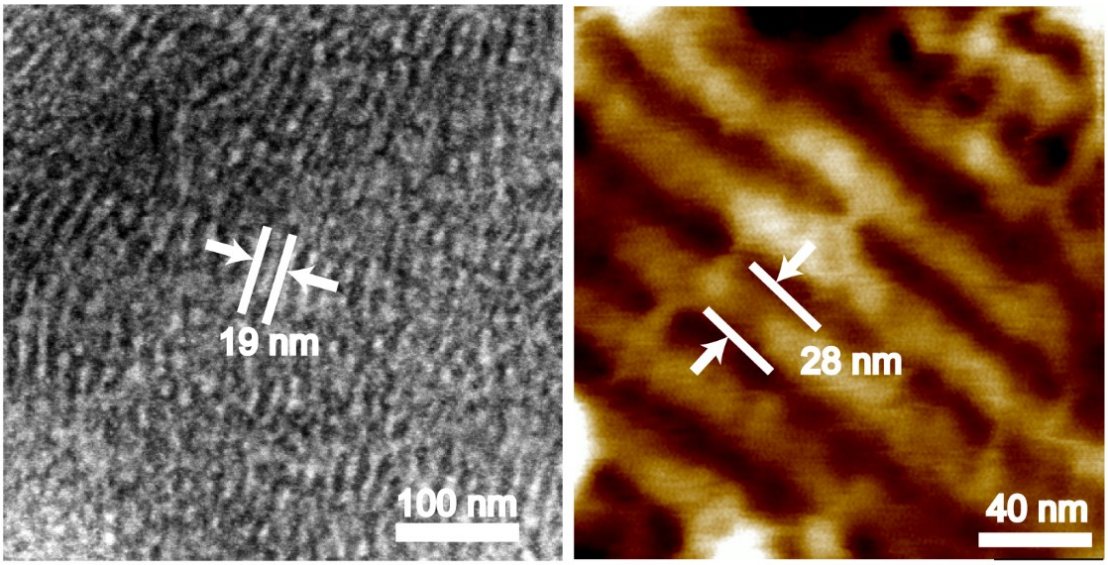

Figure S13. TEM and AFM images of LC-BCP@DiBE-DTA films.

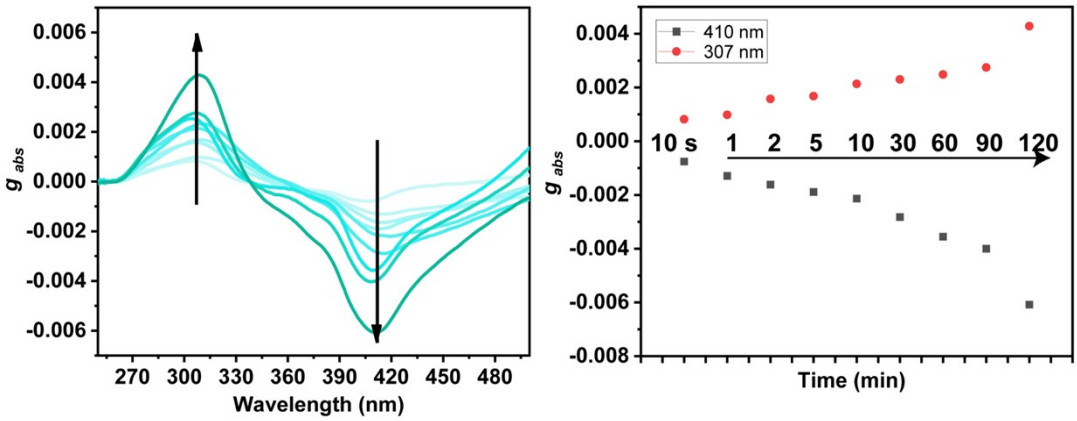

Figure S14. g_{abs} spectrum of LC-BCP@DiB-LTA.

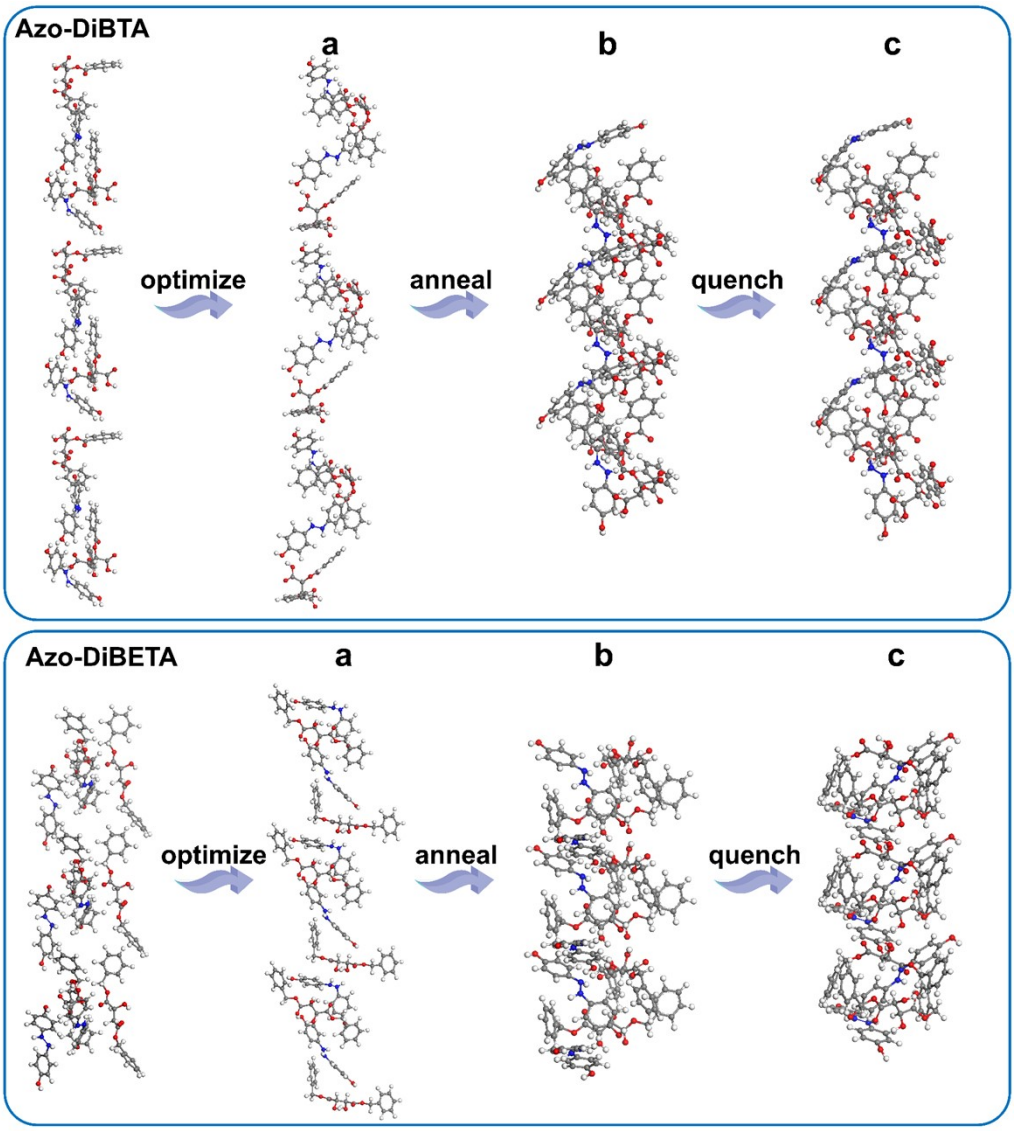

Figure S15. Energy-optimized structure (a), NVT and NPT annealing dynamic simulation (b), and quenching dynamic simulation (c).

References

1. H. Sun, Z. Jin, C. Yang, R. L. C. Akkermans, S. H. Robertson, N. A. Spenley, S. Miller and S. M. Todd, *Journal of molecular modeling*, 2016, **22**, 47.
2. Y. Fu, L. Liao, L. Yang, Y. Lan, L. Mei, Y. Liu and S. Hu, *Molecular Simulation*, 2013, **39**, 415-422.
3. D. J. Evans and B. L. Holian, *The Journal of Chemical Physics*, 1985, **83**, 4069-4074.
4. A. Abe, R. L. Jernigan and P. J. Flory, *Journal of the American Chemical Society*, 1966, **88**, 631-639.
5. Q. L. Xiong and S. A. Meguid, *European Polymer Journal*, 2015, **69**, 1-15.
6. A. Mazzanti and D. Casarini, *WIREs Computational Molecular Science*, 2012, **2**, 613-641.
7. R. S. Giri and B. Mandal, *CrystEngComm*, 2022, **24**, 10-32.